RSC Advances

ROYAL SOCIETY OF CHEMISTRY

www.rsc.org/advances

Graphics Abstract:

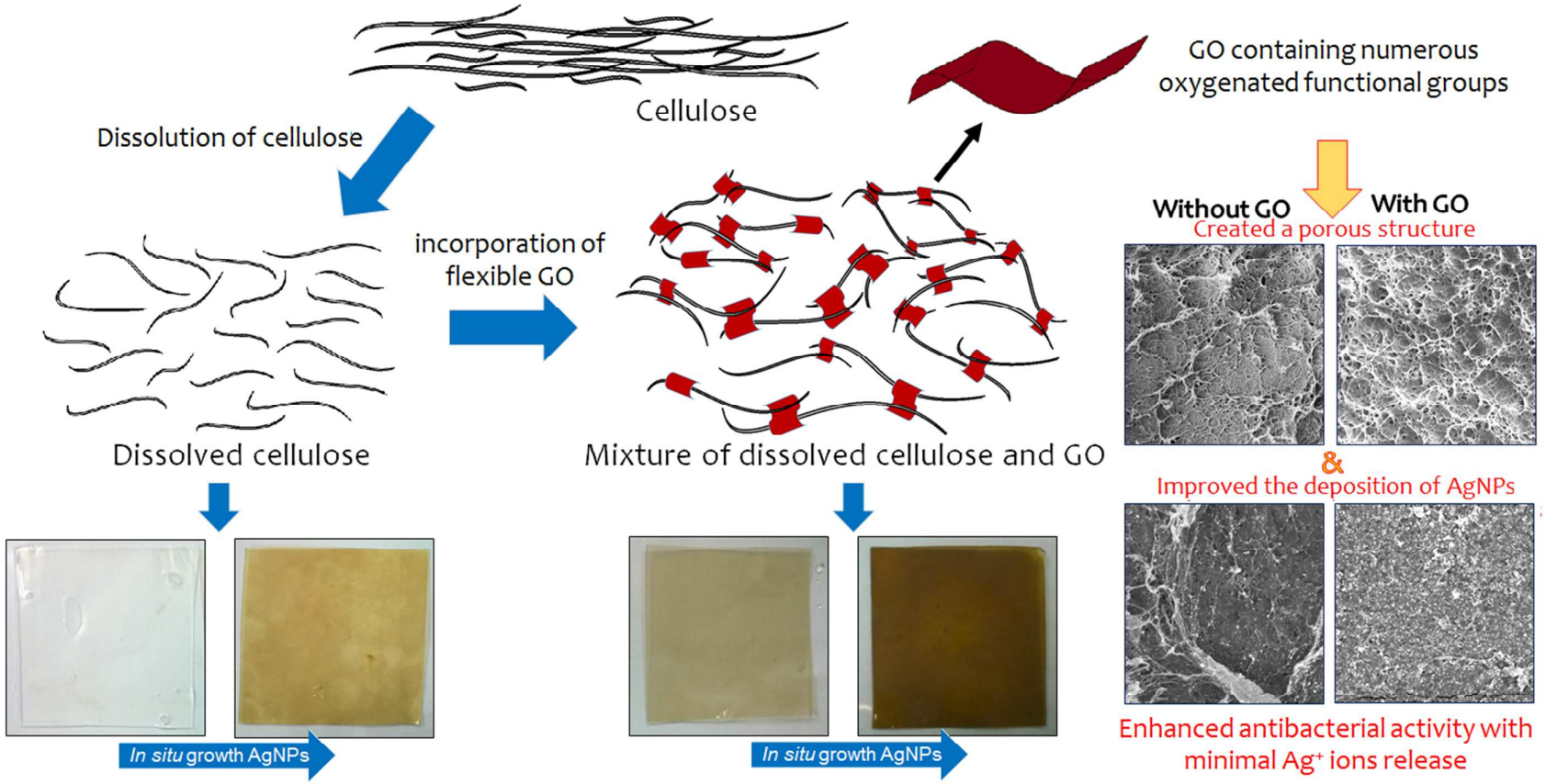

Antibacterial hybrid GO-AgNPs cellulose membrane was prepared. Incorporation of GO created a more porous structure of the regenerated cellulose membrane. GO improved the deposition of AgNPs and prevented Ag ions leaching. The composite demonstrated an effective antibacterial activity with minimal release of Ag ions.

Journal Name

RSCPublishing

ARTICLE

Antibacterial hybrid cellulose-graphene oxide nanocomposite immobilized with silver nanoparticles

Cite this: DOI: 10.1039/x0xx00000x

Received ooth January 2012,
Accepted ooth January 2012

DOI: 10.1039/x0xx00000x

www.rsc.org/

Soon Wei Chook [a], Chin Hua Chia [a*], Sarani Zakaria [a], Mohd Khan Ayob [b], Nay Ming Huang [c], Hui Min Neoh [d], Rahman Jamal [d]

A hybrid nanocomposite cellulose membrane containing graphene oxide and silver nanoparticles was produced via a two steps synthesis method. First, regenerated cellulose membranes containing different percentages of graphene oxide (GO) were produced by coagulating the mixture in an acid coagulating bath. Afterward, silver nanoparticles (AgNPs) were *in situ* synthesized onto the membranes using the modified Tollens' method. The presence of GO on the cellulose membranes significantly enhanced the deposition of AgNPs due to the electrostatic interaction between the positively charged silver ammonia complex and negatively charged oxygenated functional groups of GO before the reduction to AgNPs. The AgNPs content of the membrane with 1 wt% of GO was approximately 26 times greater than that of the neat cellulose membrane. More interestingly, the presence of GO significantly lowered the release of Ag ions and leaching of AgNPs into the aqueous solution. The produced composite membranes exhibited strong antibacterial activity against *S. aureus* and *E. coli*.

1. Introduction

For the past few decades, silver nanoparticles (AgNPs) have gained immense attention for their fascinating properties, especially their antibacterial properties against a wide range of bacteria[1]. The high surface area to volume ratio of AgNPs allows more direct contact with bacteria or more efficient Ag^+ ions release to inflict damage on bacterial components[2-4]. Despite showing great potential in various applications such as water disinfectant[5] and wound dressings[6], the implementation of AgNPs into real life applications has been limited by issues, such as the leaching of Ag particles or ions[7, 8], which has created safety and risk concerns in relation to the environment and human health[9]. Thus, several endeavours to immobilize AgNPs on substrate or supported material such as textile[10, 11], carbonaceous nanomaterials[12-14] and polymers[9, 15, 16] via *in situ* synthesis have been proposed to overcome these problems.

Cellulosic materials have often been used as a platform for nanoparticle immobilization[17-21] because of their macromolecule structure consisting of abundant reactive hydroxyl groups (-OH) which can act as the nano nucleation site for particles formation. By nature, cellulose exhibits non-specific functional properties and could be benefited with an introduction of new functionality through functionalization of nanoparticles. Among that, several works has demonstrated that the utilization of regenerated cellulose as a template to produce functional nanocomposite by incorporating various kind of nanoparticles[22-27]. Briefly, regenerated cellulose is obtained via dissolution of native cellulose, followed with regeneration process. Cellulose is non-soluble in common solutions, hence an alkaline solution composed of sodium hydroxide and urea was developed to dissolve cellulose at low temperature[28]. Cellulose dissolution provides a versatile approach that allowed cellulose to be processed into various forms, such as hydrogel[29], membrane[30], fiber[31] and aerogel[32].

Graphene oxide (GO) has emerged as one of the most studied nanomaterials in recent years. Apart from graphene, GO exhibits rather different characteristics, such as good solvent dispersity, mainly due to the presence of oxygenated functional groups. Owing to these functional groups, GO has been widely used for immobilizing numerous metallic nanoparticles[33, 34] and pollutants removal studies[35-37]. Besides, numerous studies has reported the excellent antibacterial properties of GO based materials. This including colloidal GO[38, 39], GO paper[40], GO modified cotton fabrics[41], GO-bacterial cellulose[42], AgNPs-GO nanocomposite (AgGO)[12, 43] and AgGO-polymer composites[27, 44]. Recently, several studies have demonstrated that GO is excellently compatible within cellulosic matrix, where the physical properties of the composite can be improved significantly[45-47]. Hereby, GO embedded regenerated cellulose nanocomposite membrane prepared via a feasible solution mixing and casting method, followed by the *in situ* synthesis of

AgNPs. The role of GO on the formation of AgNPs on the cellulose-GO membranes and the antibacterial activity of the membranes against *Staphylococcus aureus* (*S. aureus*) *and Escherichia coli* (*E. coli*) were investigated. The release or leaching of the Ag^+ ions of the membranes was also studied.

2. Experimental

2.1. Materials and chemicals

Cotton linter was supplied by Hubei Chemical Fiber Co. Ltd. (Xiangfan, China) with a weight-average molecular weight (M_w) of 9.0 × 104, as determined by static laser light scattering (DAWN DSP, Wyatt Technology Co., USA). Silver nitrate ($AgNO_3$), sodium hydroxide (NaOH), ammonium hydroxide (NH_4OH, 25%), potassium permanganate ($KMnO_4$, 99.9%), hydrogen peroxide (H_2O_2, 30%), sulphuric acid (H_2SO_4, 98%) and phosphoric acid (H_3PO_4, 85%) were purchased from Merck (Darmstadt, Germany). Glucose and urea were purchased from Sigma Aldrich. Graphite flake was purchased from Asbury Graphite Mill, Inc. (Asbury, NJ, USA). All the chemicals were analytical grade and used without further purification.

2.2. Preparation of GO

GO was prepared using the simplified Hummer's method[48]. First, the graphite flake was oxidized to graphite oxide with H_2SO_4 and $KMnO_4$ by stirring the mixture for 3 days. In order to stop the oxidation reaction, H_2O_2 was added into the graphite oxide solution, which was followed by centrifugation to remove the excess chemicals. The graphite oxide was washed repeatedly and then placed in an ultra-sonication bath to obtain exfoliated graphene oxide.

2.3. *In situ* preparation of AgNPs on GO-embedded regenerated cellulose membrane

Cotton linter fiber was added to a precooled (–12 °C) aqueous solution of NaOH/urea (7.0 wt% /12.0 wt%), and stirred vigorously at room temperature until a transparent cellulose solution (4.0 wt%) was obtained after centrifugation. A plain membrane without GO was prepared and labelled as CM. Three GO-cellulose solution mixtures containing 0.25, 0.50 and 1.00 wt% of GO were produced and regenerated in a 5 wt% acetic acid coagulation bath. These were labelled CMGO1, CMGO2, and CMGO3, respectively. The membranes were collected and washed repeatedly with DI water to remove excess chemicals. Each membranes with a same dimension of 5 × 5 cm was immersed into a solution containing silver ammonia complex, $Ag(NH_3)_2^+$, separately. After 30 min, glucose was added to induce the formation of AgNPs under microwave irradiation for 1 min.

2.4. Characterizations

The X-ray diffraction pattern of each membrane was obtained using an X-ray diffractometer (XRD, Bruker Advance). The dried membranes were observed under a field emission scanning electron microscope (FESEM, LEO 1450VP) using SE2 and backscattering mode. FESEM sample preparation was carried out by froze the membrane using liquid nitrogen and freeze dried overnight. Furthermore, the membrane sample was immersed in a 10 wt% of nitric acid and DI water for 4 h and continuously shaken at 120 rpm. Both solutions were withdrawn and further diluted to measure the AgNPs content and Ag ions release using inductively coupled plasma-optical emission spectroscopy (ICP-OES, Perkin Elmer Optima 4300 DV). X-ray photoelectron (XPS) spectra of the CM-Ag and CMGO3-Ag was obtained using a high resolution Auger electron spectroscopy with XPS (AES-XPS, Kratos Shidmazu).

2.5. Antibacterial Test

CM-Ag and CMGO-Ag membranes were cut into five sheets with the dimensions of 2 cm × 1 cm and immersed into nutrient broth inoculated with 10^5 CFU/mL of both *S. aureus* and *E. coli*, respectively. Control containing bacterial inoculated broth was prepared without a membrane. The samples were incubated in an incubator shaker at 37 °C at 120 rpm for 4 h. Then, the OD600 values for the control (OD_c) and samples (OD_s) were obtained at 600 nm. The antibacterial performance was calculated based on the equation depicted in Equation (1).

$$\text{Inhibition rate (\%)} = [1 - OD_s/OD_c] \times 100\ \% \quad (1)$$

3. Results and Discussion

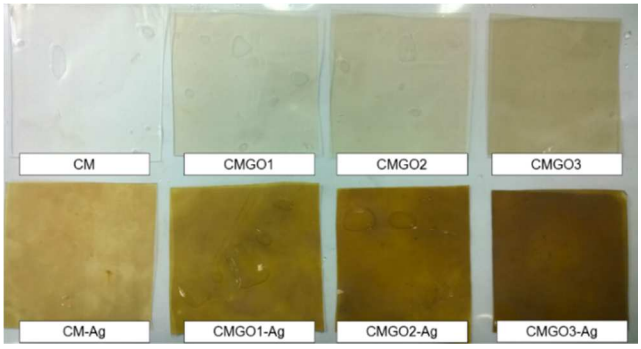

Fig. 1 Digital images of membranes before and after *in situ* synthesis of AgNPs.

Visual observations of the CM and CMGO before and after the *in situ* growth of AgNPs were captured digitally and are depicted in Fig. 1. The GO was observably well distributed within the regenerated cellulose without obvious aggregations. The membranes has further transformed into yellowish colour as an indication of the AgNPs formation on the membranes.

As shown in Fig. 2, a diffraction pattern of cellulose II was recorded for all the samples at the peak of 12°, 20° and 22°, proving the accomplishment of the dissolution and regeneration

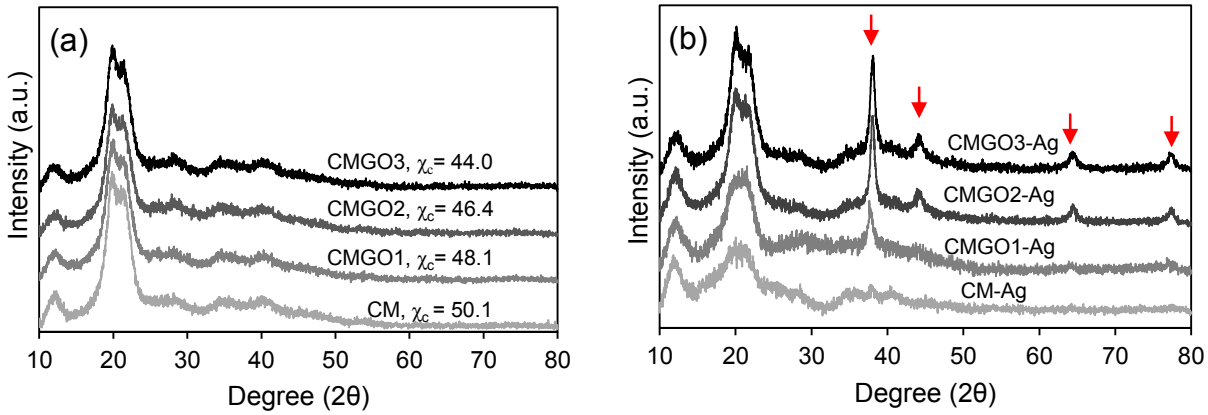

Fig. 2 XRD diffraction pattern for CM and CMGO (a) before and (b) after the synthesis of AgNPs.

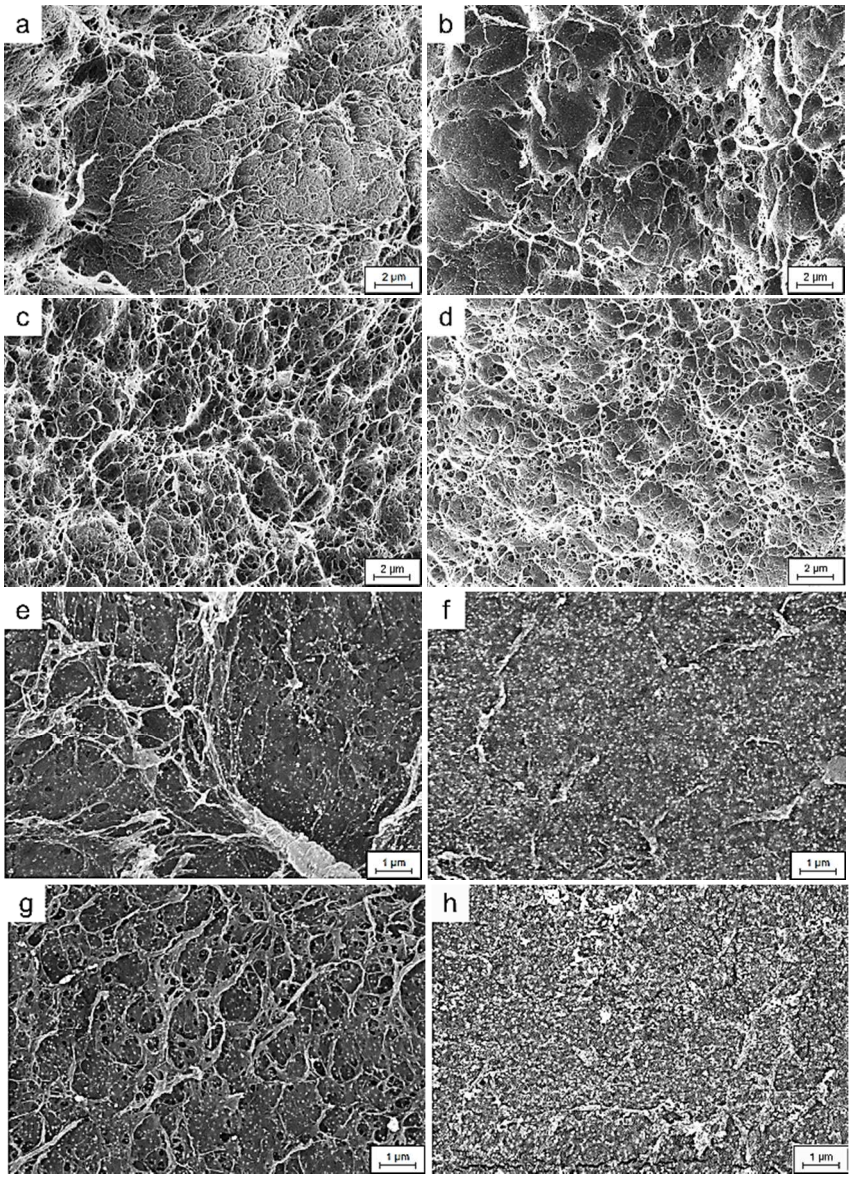

Fig. 3 Surface morphologies of (a) CM-Ag and (b) CMGO1-Ag, (c) CMGO2-Ag and (d) CMGO3-Ag; distribution of AgNPs on (e) CM-Ag, (f) CMGO1-Ag, (g) CMGO2-Ag and (h) CMGO3-Ag.

of cellulose. As depicted in Fig. 2a, the calculated degree of crystallinity (χ_c) for the samples has decreased from 50.1 to 44.0 as the GO content increased, which may have been due to the incorporation of GO interrupting the rearrangement of cellulose crystals during the regeneration process[46]. On the other hand, the XRD diffraction pattern of the membrane after the immobilization of the AgNPs (Fig. 2b) revealed the successful formation of crystallite AgNPs, where a significant peak (indicated by the red arrow) corresponding to the Ag crystal (No. JCPDS: 04-0783) was found for each sample.

The membranes surface structure was observed under FESEM, and the images are shown in Fig. 3. Obvious physical structure changes with the incorporation of the GO can be observed, with the CMGO-Ag samples (Fig. 3b–3d) exhibiting a more porous structure compared to the denser structure of CM-Ag (Fig. 3a). The formation of intermolecular hydrogen bonds between the GO and dissolved cellulose was accounted for the transformation, where the insertion of the flexible GO has disrupted the regeneration of the cellulose network[46], as depicted in Fig. 4. The formation of AgNPs was confirmed using the backscattered mode of SEM (Fig. 3e–3h), where an increased distribution of AgNPs as white spots can be observed on the surface of membranes.

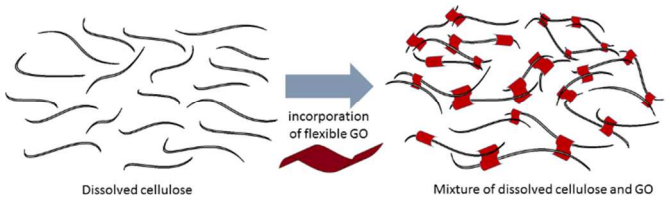

Fig. 4 Schematic illustration of interactions between dissolved cellulose and GO via intermolecular hydrogen bonding.

Table 1 ICP-OES determination of AgNPs content and Ag^+ release for CM-Ag and CMGO-Ag

Sample	GO content (wt%)	ICP-OES Measurement	
		AgNPs content ($\mu g/cm^2$)	Ag^+ ions release ($\mu g/mL$)
CM-Ag	-	0.75	0.85
CMGO1-Ag	0.25	7.88	0.98
CMGO2-Ag	0.50	14.95	0.76
CMGO3-Ag	1.00	20.00	0.56

The AgNPs content of the membranes and Ag^+ ions released, as measured using ICP-OES, are listed in Table 1. The AgNPs content of the membranes increased as the amount of embedded GO increased. First, $Ag(NH_3)_2^+$ was allowed to diffuse through the porous structure of the CMGO with the immersion into $Ag(NH_3)_2^+$ solution. The positively charged $Ag(NH_3)_2^+$ was electrostatically attracted toward the negatively charged oxygen functional groups available on CMGO, in which GO introduced extra available oxygen functional groups. With the introduction of glucose under the condition of microwave irradiation, $Ag(NH_3)_2^+$ was immediately reduced to zero valence Ag^0 nuclei which deposited and continuously grew into crystalline AgNPs on the membrane surface.

Interestingly, the amount of Ag^+ ions released from the membranes decreased despite the increase in the AgNPs content from CMGO1 to CMGO3. The Ag^+ ions release rate was calculated considering the total amount of Ag ions released to the total amount of AgNPs present on the membranes. The Ag^+ ions release rates of CM-Ag, CMGO1-Ag, CMGO2-Ag and CMGO3-Ag were 34.1%, 3.7%, 1.5% and 0.84%, respectively. The significant reduction in the Ag^+ ion release rate could be due to the increase in the GO-AgNPs interaction, which enhanced the stability of the AgNPs and rendered the oxidative dissolution of Ag^+ ions. The XPS results shown in Fig. 5 revealed that both samples contained a characteristic Ag 3d spectrum with a spin orbit splitting value of 6.0 eV. In particular, CM-Ag (Fig. 5a) had a lower binding energy Ag 3d (367.9 eV and 373.9eV) compared to the pure Ag standard (368.2 eV and 374.2 eV) and CMGO3-Ag (368.1 eV and 374.1 eV), as shown in Fig. 5b. This indicated that the AgNPs of CM-Ag underwent greater oxidation that led to the oxidative dissolution of Ag^+ ions, which explained the higher release rate of CM-Ag compared to CMGO-Ag[3, 49]. Commonly, positive shift of binding energy for metal upon oxidation was observed due to the electronegativity difference. However, the binding energy of Ag 3d in this study underwent a negative shift upon oxidation is similar to several reported studies[50-52], which can be attributed to other factors such as lattice potential, work function changes and extra-atomic relaxation energy[53].

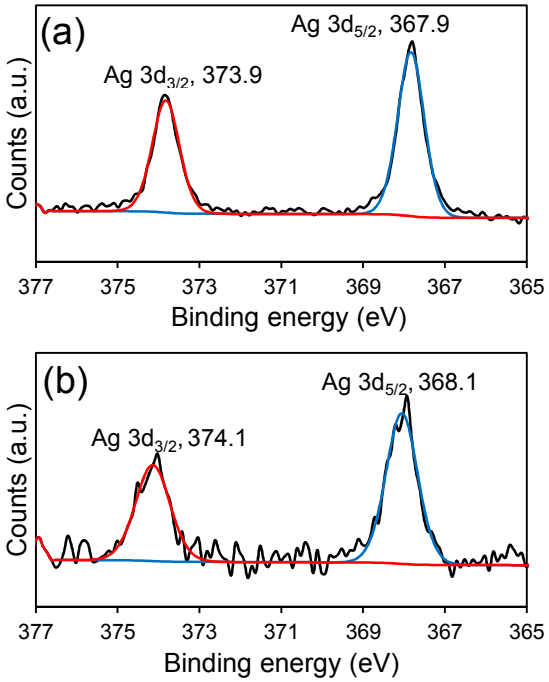

Fig. 5 High resolution XPS spectra of Ag 3d for (a) CM-Ag and (b) CMGO3-Ag.

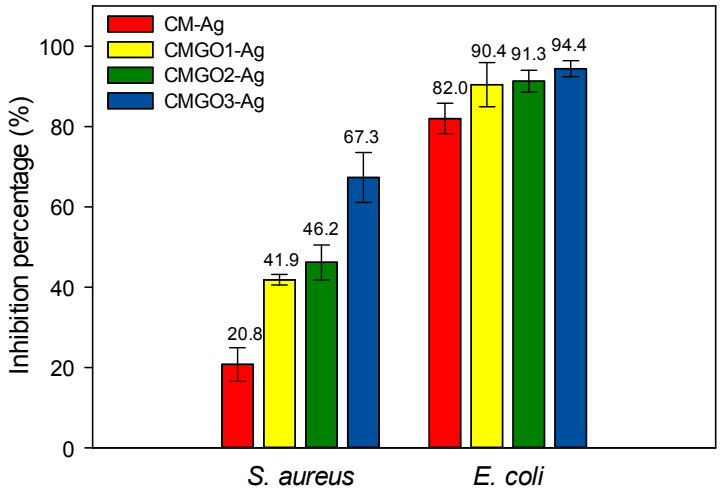

Fig. 6 Antibacterial activities of CM-Ag and CMGO-Ag against *S. aureus* and *E .coli.*

The antibacterial activity of the CMGO-Ag is presented in Fig. 6. In general, the antibacterial activities of the nanocomposite membranes produced with higher amounts of AgNPs were more effective at inhibiting the growth of both *S. aureus* and *E. coli*. Albeit it had the highest release rate of Ag^+ ions, CM-Ag exhibited the weakest antibacterial activity against both bacteria due to its low AgNPs content. In contrast, CMGO-Ag membranes with higher AgNPs contents and lower Ag ions released showed better antibacterial performance, especially against *S. aureus*. In addition, it is important to note that the porous structure of the CMGO-Ag membranes permitted the bacteria to diffuse through, which facilitated more direct interaction with the AgNPs deposited on the structure. In contrast, CM and CMGO exhibited non-effective antibacterial activity without the presence of AgNPs (Fig. S3). By combining the obtained results, we suggest that the strong inhibition effect of the CMGO-Ag membranes could mainly be attributed to the direct contact between the nanoparticles and bacteria, instead of the released Ag^+ ions.

4. Conclusions

In summary, this work demonstrated that the dissolution of cellulose has provided an advantage for cellulose to be processable and improved its functionality by incorporating GO during regeneration process. The surface functionality of the GO-embedded regenerated cellulose membranes was significantly improved as compared to the neat membrane, where the deposition of AgNPs can be significantly enhanced with the increase of GO content. In return, the GO-embedded membranes showed an effective bacterial inhibition effect with a minimal Ag^+ ion release, in which the membrane's porous structure improved the interactions between bacteria and AgNPs. Given these advantages, the produced membrane is envisioned to be applicable for wound dressing and wastewater disinfection applications. The practical or realization of the membranes in those area of application should be further accessed to fully understand the performance of the membranes, which would involve complicated factors and conditions.

Acknowledgements

The authors acknowledge the financial support provided by the research project grants of DIP-2014-013 and LRGS/TD/2012/USM-UKM/PT/04. N. M. Huang acknowledges obtaining a High Impact Research Grant from the Ministry of Higher Education of Malaysia (UM.C/P/HIR/MOHE/SC/21). S. W. Chook appreciates Prof. Dr. Lina Zhang for her kind support at Wuhan University.

Notes

[a] School of Applied Physics, Faculty of Science and Technology, Universiti Kebangsaan Malaysia, 43600 UKM Bangi, Selangor, Malaysia
[b] School of Chemical Sciences and Food Technology, Faculty of Science and Technology, Universiti Kebangsaan Malaysia, 43600 UKM Bangi, Selangor, Malaysia
[c] Physics Department, Faculty of Science, University of Malaya, 50603 Kuala Lumpur, Malaysia
[d] UKM Medical Molecular Biology Institute, Universiti Kebangsaan Malaysia,56000 Cheras, Kuala Lumpur, Malaysia,.
*e-mail: chiachinhua@yahoo.com/ chia@ukm.edu.my

Electronic Supplementary Information (ESI) available: [The FTIR and Raman spectrum of the samples were included in the ESI file]. See DOI: 10.1039/b000000x/

References

1. M. Rai, A. Yadav and A. Gade, *Biotechnol. Adv.*, 2009, **27**, 76-83.

2. S. Agnihotri, S. Mukherji and S. Mukherji, *Nanoscale*, 2013, **5**, 7328-7340.
3. Z.-m. Xiu, Q.-b. Zhang, H. L. Puppala, V. L. Colvin and P. J. J. Alvarez, *Nano Lett*, 2012, **12**, 4271-4275.
4. G. A. Sotiriou and S. E. Pratsinis, *Environ. Sci. Technol.*, 2010, **44**, 5649-5654.
5. X. Wang, Y. Dai, J.-l. Zou, L.-y. Meng, S. Ishikawa, S. Li, M. Abuobeidah and H.-g. Fu, *RSC Adv.*, 2013, **3**, 11751-11758.
6. B. S. Atiyeh, M. Costagliola, S. N. Hayek and S. A. Dibo, *Burns*, 2007, **33**, 139-148.
7. X. Li and J. J. Lenhart, *Environ. Sci. Technol.*, 2012, **46**, 5378-5386.
8. C.-N. Lok, C.-M. Ho, R. Chen, Q.-Y. He, W.-Y. Yu, H. Sun, P.-H. Tam, J.-F. Chiu and C.-M. Che, *JBIC, J. Biol. Inorg. Chem.*, 2007, **12**, 527-534.
9. Y. Cheng, L. Yin, S. Lin, M. Wiesner, E. Bernhardt and J. Liu, *J. Phys. Chem. C*, 2011, **115**, 4425-4432.
10. B. H. Dong and J. P. Hinestroza, *ACS Appl. Mater. Interfaces*, 2009, **1**, 797-803.
11. I. Osório, R. Igreja, R. Franco and J. Cortez, *Mater. Lett.*, 2012, **75**, 200-203.
12. S. Chook, C. Chia, S. Zakaria, M. Ayob, K. Chee, N. Huang, H. Neoh, H. Lim, R. Jamal and R. Rahman, *Nanoscale Res. Lett.*, 2012, **7**, 541.
13. C.-H. Xue, R.-J. Zhou, M.-M. Shi, Y. Gao, G. Wu, X.-B. Zhang, H.-Z. Chen and M. Wang, *Nanotechnology*, 2008, **19**, 325605.
14. C. Tang, W. Sun and W. Yan, *RSC Adv.,* 2014, **4**, 523-530.
15. W. D. Cook, Q. D. Nghiem, Q. Chen, F. Chen and M. Sangermano, *Macromolecules*, 2011, **44**, 4065-4071.
16. S. Gupta, P. Uhlmann, M. Agrawal, S. Chapuis, U. Oertel and M. Stamm, *Macromolecules*, 2008, **41**, 2874-2879.
17. H. Dong, J. F. Snyder, D. T. Tran and J. L. Leadore, *Carbohydr. Polym.*, 2013, **95**, 760-767.
18. G. Yang, J. Xie, F. Hong, Z. Cao and X. Yang, *Carbohydr. Polym.,* 2012, **87**, 839-845.
19. E. Smiechowicz, P. Kulpinski, B. Niekraszewicz and A. Bacciarelli, *Cellulose*, 2011, **18**, 975-985.
20. H. Liu, D. Wang, Z. Song and S. Shang, *Cellulose*, 2011, **18**, 67-74.
21. J. You, M. Xiang, H. Hu, J. Cai, J. Zhou and Y. Zhang, *RSC Adv.*, 2013, **3**, 19319-19329.
22. J. Cai, S. Kimura, M. Wada and S. Kuga, *Biomacromolecules*, 2008, **10**, 87-94.
23. S. Hribernik, M. S. Smole, K. S. Kleinschek, M. Bele, J. Jamnik and M. Gaberscek, *Polym. Degrad. Stab.*, 2007, **92**, 1957-1965.
24. A. John, H.-U. Ko, D.-G. Kim and J. Kim, *Cellulose*, 2011, **18**, 675-680.
25. Z. Liu, M. Li, L. Turyanska, O. Makarovsky, A. Patanè, W. Wu and S. Mann, *Chem. Mater.*, 2010, **22**, 2675-2680.
26. J. Wu, N. Zhao, X. Zhang and J. Xu, *Cellulose*, 2012, **19**, 1239-1249.
27. S. Chook, C. Chia, S. Zakaria, M. Ayob, N. Huang, H. Neoh, M. He, L. Zhang and R. Jamal, *Cellulose*, 2014, **21**, 4261-4270.
28. X. Luo and L. Zhang, *Food Res. Int.,* 2013, **52**, 387-400.
29. C. Chang, S. Chen and L. Zhang, *J. Mater. Chem.*, 2011, **21**, 3865-3871.
30. H. Kaco, S. Zakaria, C. H. Chia and L. Zhang, *Bioresouces*, 2014, **9**, 2167-2178.
31. G. Jiang, W. Huang, L. Li, X. Wang, F. Pang, Y. Zhang and H. Wang, *Carbohydr. Polym.,* 2012, **87**, 2012-2018.
32. J. Cai, S. Kimura, M. Wada, S. Kuga and L. Zhang, *ChemSusChem*, 2008, **1**, 149-154.
33. X. Wang, P. Huang, L. Feng, M. He, S. Guo, G. Shen and D. Cui, *RSC Adv.*, 2012, **2**, 3816-3822.
34. A. M. Golsheikh, N. M. Huang, H. N. Lim and R. Zakaria, *RSC Adv.*, 2014, **4**, 36401-36411.
35. C. H. Chia, N. F. Razali, M. S. Sajab, S. Zakaria, N. M. Huang and H. N. Lim, *Sains Malays.,* 2013, **42**, 819-826.
36. S.-T. Yang, S. Chen, Y. Chang, A. Cao, Y. Liu and H. Wang, *J. Colloid Interface Sci.*, 2011, **359**, 24-29.
37. X. Yang, C. Chen, J. Li, G. Zhao, X. Ren and X. Wang, *RSC Adv.*, 2012, **2**, 8821-8826.
38. L. Hui, J.-G. Piao, J. Auletta, K. Hu, Y. Zhu, T. Meyer, H. Liu and L. Yang, *ACS Appl. Mater. Interfaces*, 2014, **6**, 13183-13190.
39. S. Liu, T. H. Zeng, M. Hofmann, E. Burcombe, J. Wei, R. Jiang, J. Kong and Y. Chen, *ACS Nano*, 2011, **5**, 6971-6980.
40. W. Hu, C. Peng, W. Luo, M. Lv, X. Li, D. Li, Q. Huang and C. Fan, *ACS Nano*, 2010, **4**, 4317-4323.
41. J. Zhao, B. Deng, M. Lv, J. Li, Y. Zhang, H. Jiang, C. Peng, J. Li, J. Shi, Q. Huang and C. Fan, *Adv. Healthcare Mater.*, 2013, **2**, 1259-1266.
42. W. Shao, H. Liu, X. Liu, S. Wang and R. Zhang, *RSC Adv.*, 2015, **5**, 4795-4803.
43. S. Barua, S. Thakur, L. Aidew, A. K. Buragohain, P. Chattopadhyay and N. Karak, *RSC Adv.*, 2014, **4**, 9777-9783.
44. Z. Fan, B. Liu, J. Wang, S. Zhang, Q. Lin, P. Gong, L. Ma and S. Yang, *Adv. Funct. Mater.*, 2014, **24**, 3933-3943.
45. M. Tian, L. Qu, X. Zhang, K. Zhang, S. Zhu, X. Guo, G. Han, X. Tang and Y. Sun, *Carbohydr. Polym.,* 2014, **111**, 456-462.
46. W. Ouyang, J. Sun, J. Memon, C. Wang, J. Geng and Y. Huang, *Carbon*, 2013, **62**, 501-509.
47. J. Zhang, Y. Cao, J. Feng and P. Wu, *J. Phys. Chem. C*, 2012, **116**, 8063-8068.
48. N. M. Huang, H. N. Lim, C. H. Chia, M. A. Yarmo and M. R. Muhamad, *Int. J. Nanomed.*, 2011, **6**, 3443-3448.
49. P. Prieto, V. Nistor, K. Nouneh, M. Oyama, M. Abd-Lefdil and R. Díaz, *Appl. Surf. Sci.*, 2012, **258**, 8807-8813
50. C. Y. Dong, D. S. Shang, L. Shi, J. R. Sun, B. G. Shen, F. Zhuge, R. W. Li and W. Chen, *Appl. Phys. Lett.,* 2011, **98**, -.
51. T. C. R. Rocha, A. Oestereich, D. V. Demidov, M. Havecker, S. Zafeiratos, G. Weinberg, V. I. Bukhtiyarov, A. Knop-Gericke and R. Schlogl, *Phys. Chem. Chem. Phys.*, 2012, **14**, 4554-4564.
52. T. C. Kaspar, T. Droubay, S. A. Chambers and P. S. Bagus, *J. Phys. Chem. C,* 2010, **114**, 21562-21571.
53. J. F. Weaver and G. B. Hoflund, *J. Phys. Chem.*, 1994, **98**, 8519-8524.